Supporting Information

Self-Assembled Nano-Composite Perovskites as Highly Efficient and Robust Hybrid Cathode for Solid Oxide Fuel Cell

Jun Hyuk Kim[a], Kyuseon Jang[a], Dae-Kwang Lim[a], Sejong Ahn[a], DongHwan Oh[a], Hyunseung Kim[a], Jongsu Seo[a], Pyuck-Pa Choi[a] and WooChul Jung[a,*]

[a] Department of Materials Science and Engineering, KAIST, Daejeon, Republic of Korea

[*]e-mail : wcjung@kaist.ac.kr

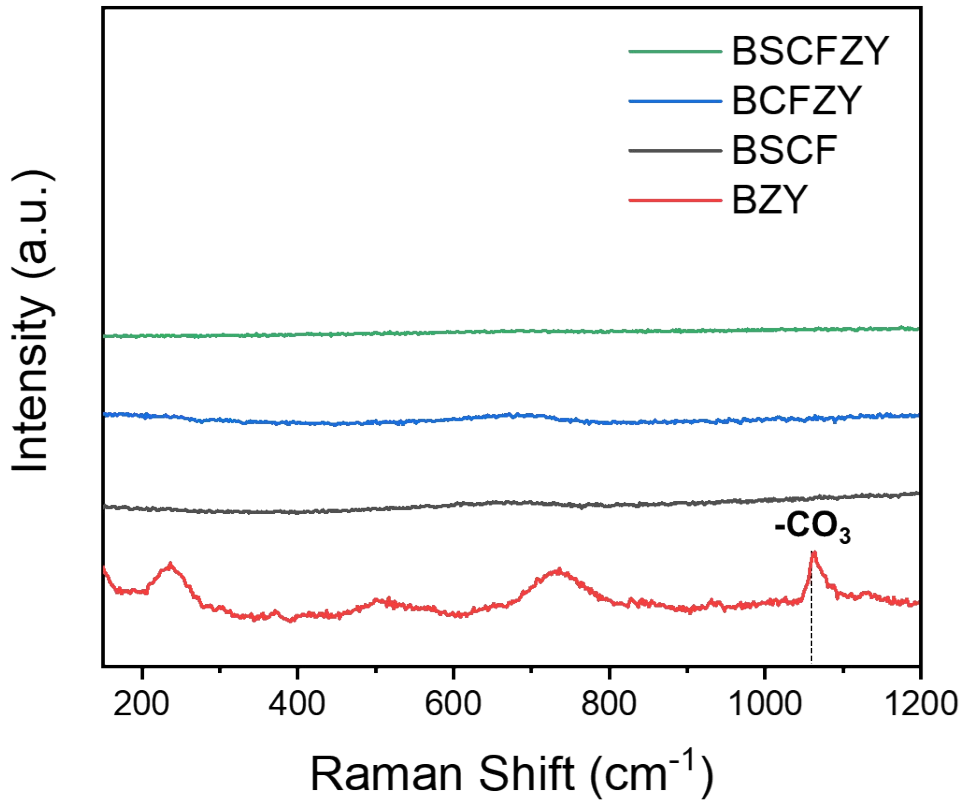

Figure S1. Raman spectra of $Ba_{0.5}Sr_{0.5}Co_{0.6}Fe_{0.2}Zr_{0.1}Y_{0.1}O_{3-\delta}$ (BSCFZY), $BaCo_{0.4}Fe_{0.4}Zr_{0.1}Y_{0.1}O_{3-\delta}$ (BCFZY), $Ba_{0.5}Sr_{0.5}Co_{0.8}Fe_{0.2}O_{3-\delta}$ (BSCF), and $BaZr_{0.8}Y_{0.2}O_{3-\delta}$ (BZY).

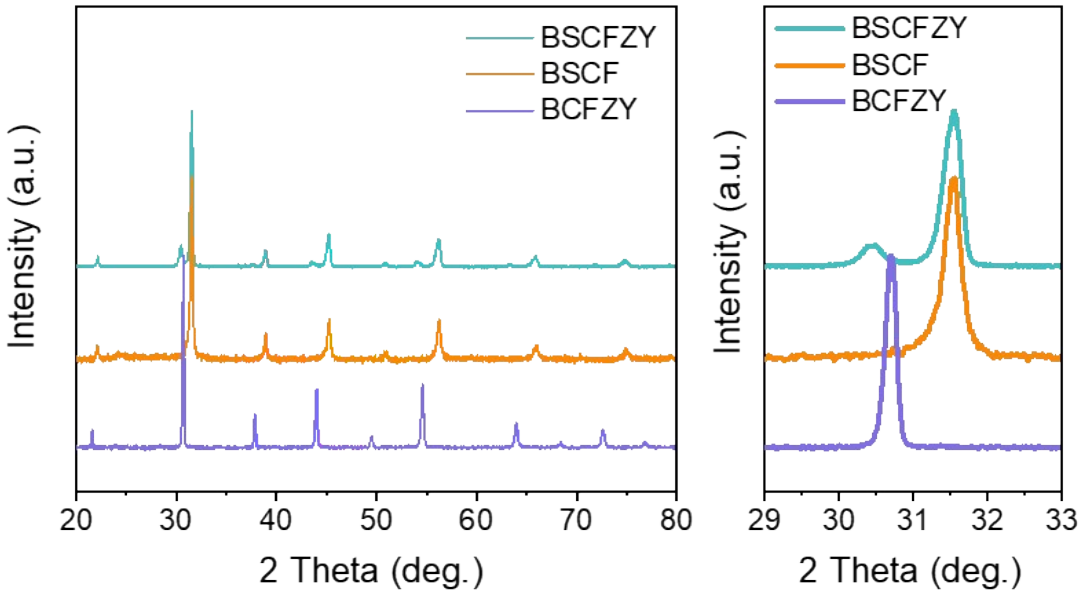

Figure S2. X-ray diffraction patterns of $Ba_{0.5}Sr_{0.5}Co_{0.6}Fe_{0.2}Zr_{0.1}Y_{0.1}O_{3-\delta}$ (BSCFZY), $BaCo_{0.4}Fe_{0.4}Zr_{0.1}Y_{0.1}O_{3-\delta}$ (BCFZY), $Ba_{0.5}Sr_{0.5}Co_{0.8}Fe_{0.2}O_{3-\delta}$ (BSCF).

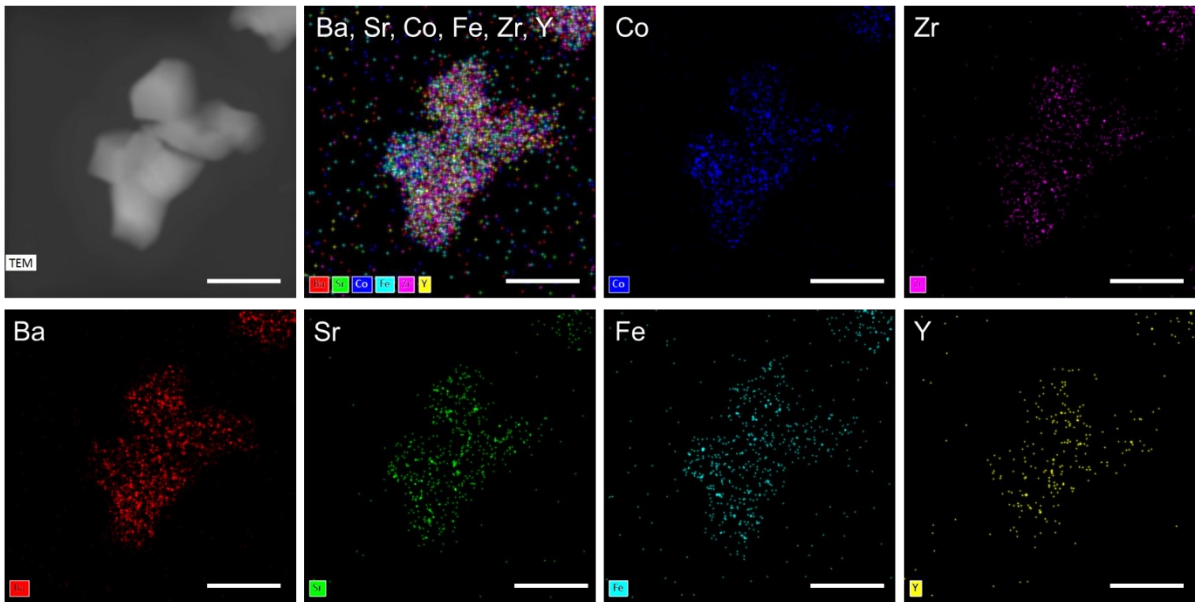

Figure S3. Scanning transmission electron microscopy (STEM) and energy-dispersive X-ray (EDX) analysis of $Ba_{0.5}Sr_{0.5}Co_{0.6}Fe_{0.2}Zr_{0.1}Y_{0.1}O_{3-\delta}$ (BSCFZY) composite. Scale bar = 50 nm.

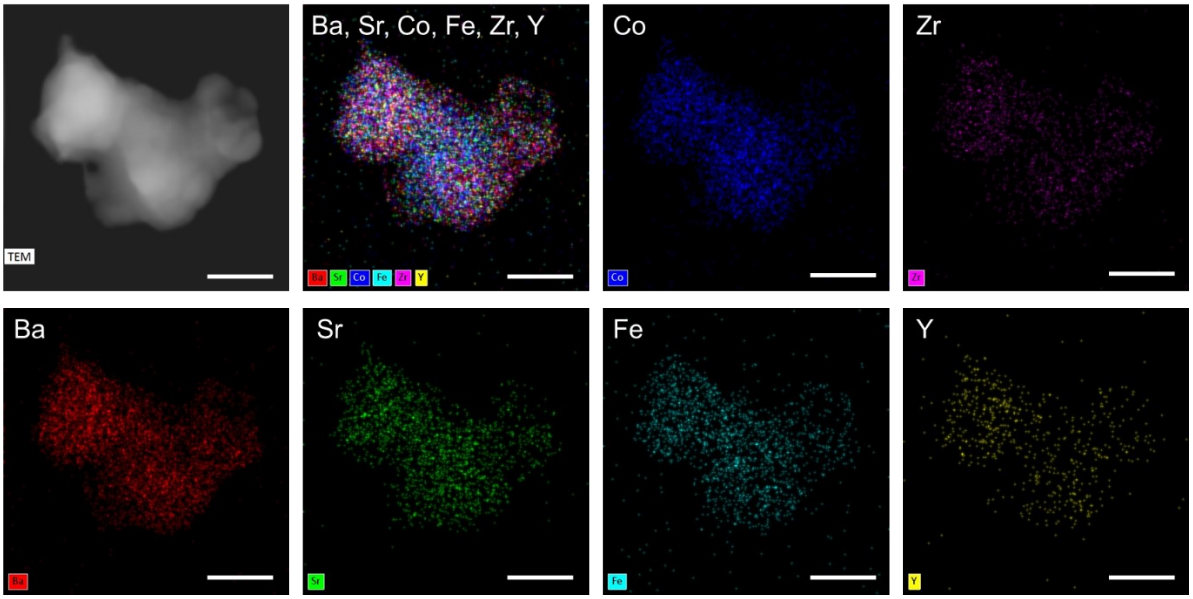

Figure S4. Scanning transmission electron microscopy (STEM) and energy-dispersive X-ray (EDX) analysis of $Ba_{0.5}Sr_{0.5}Co_{0.6}Fe_{0.2}Zr_{0.1}Y_{0.1}O_{3-\delta}$ (BSCFZY) composite. Scale bar = 90 nm.

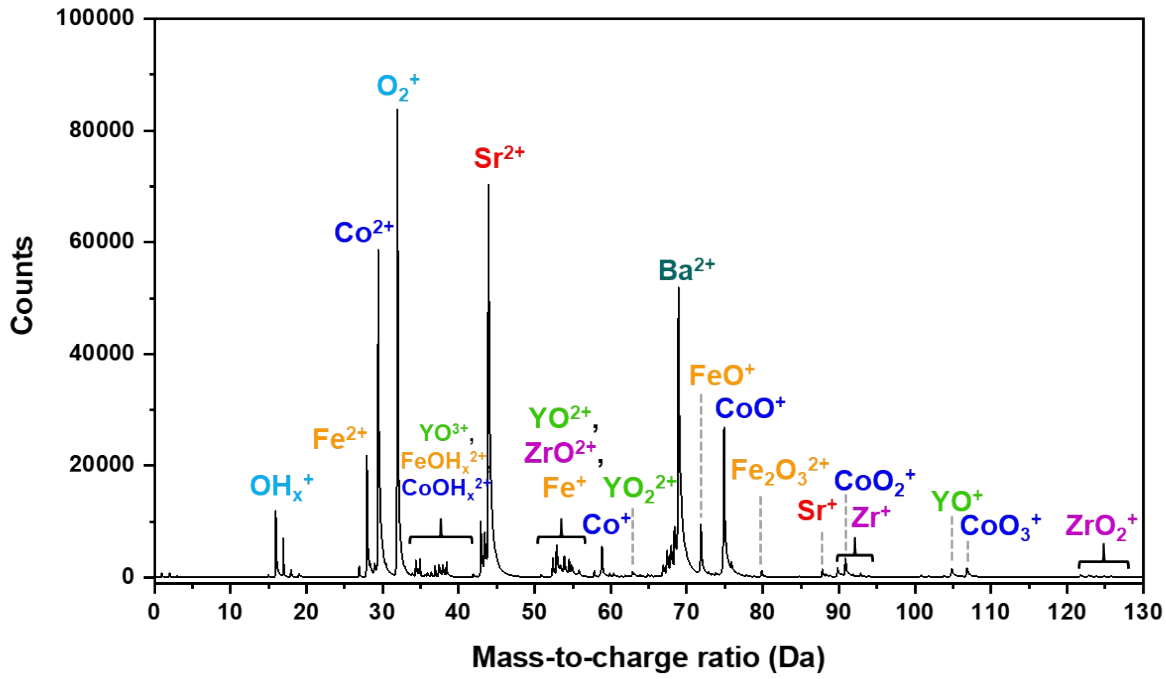

Figure S5. Mass spectrum of the BSCFZY specimen. Since the BSCFZY powder was located at the top of Ni electrodeposition layer, almost pure BSCFZY was analyzed at the first stage of APT analysis without Ni, as shown in the spectrum. All the major peaks can be assigned to ionic species related to the elements in BSCFZY. To obtain the reliability of quantitative analysis in APT, we applied the same peak ranging method (ranging at full-width at half maximum) to all the peaks in the spectrum.

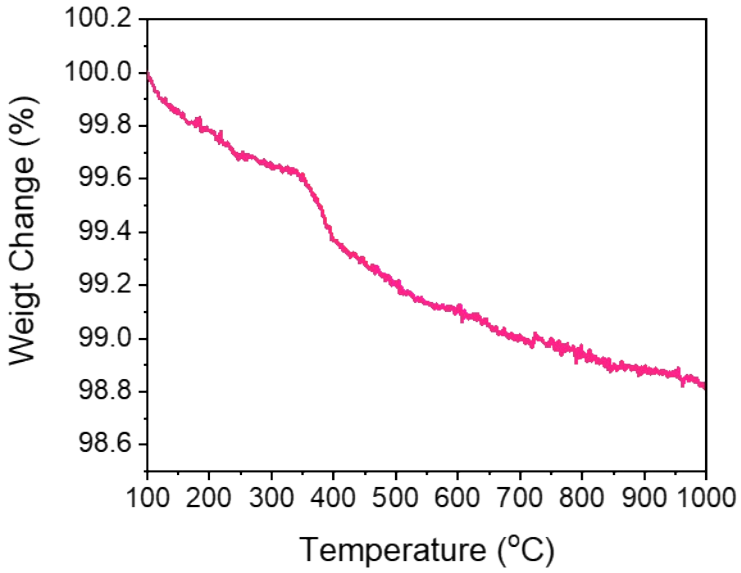

Figure S6. Thermogravimetric profiles of $Ba_{0.5}Sr_{0.5}Co_{0.6}Fe_{0.2}Zr_{0.1}Y_{0.1}O_{3-\delta}$ (BSCFZY) composite in air.

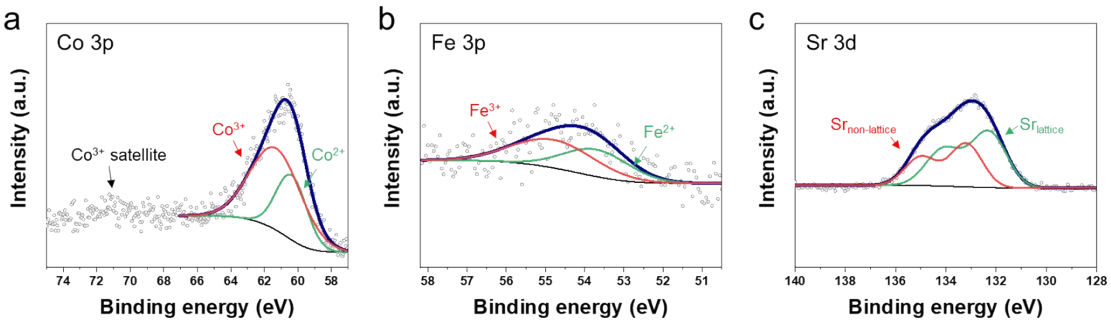

Figure S7. XPS spectra of (a) Co 3p, (b) Fe 3p, and (c) Sr 3d for BSCFZY

Table S1. Summary of the cation ratios in BSCFZY

Co		**Fe**		**Sr**	
Co^{3+}	Co^{2+}	Fe^{3+}	Fe^{2+}	$Sr_{non\text{-}lattice}$	$Sr_{lattice}$
68%	32%	57%	43%	29%	71%

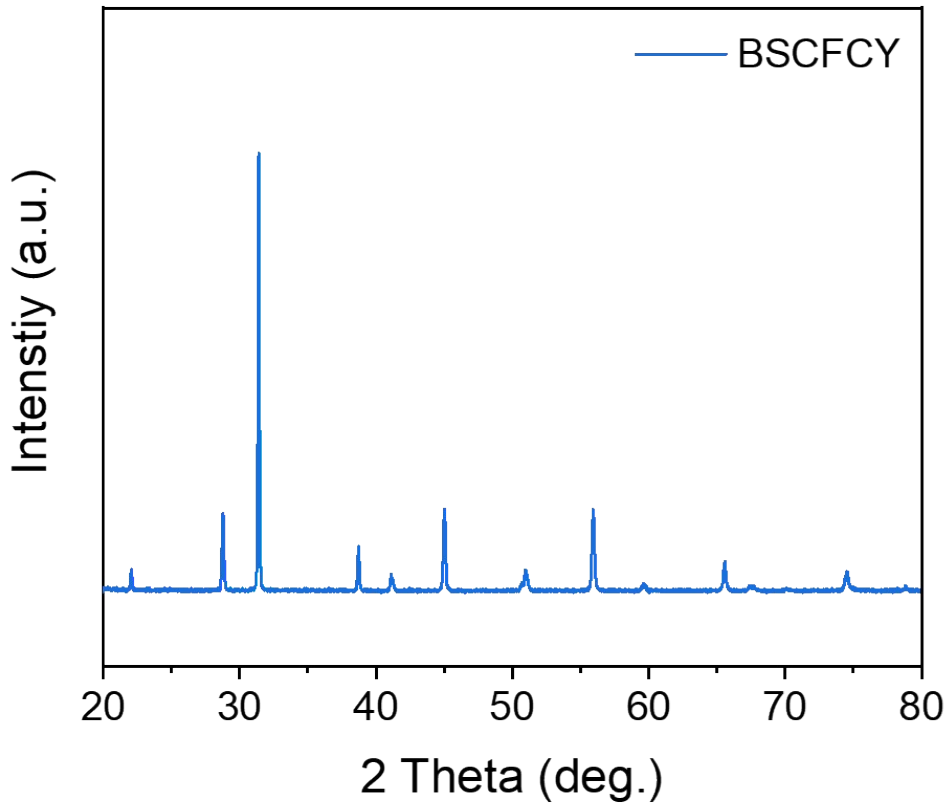

Figure S8. X-ray diffraction patterns of $Ba_{0.5}Sr_{0.5}Co_{0.6}Fe_{0.2}Ce_{0.1}Y_{0.1}O_{3-\delta}$ (BSCFCY)

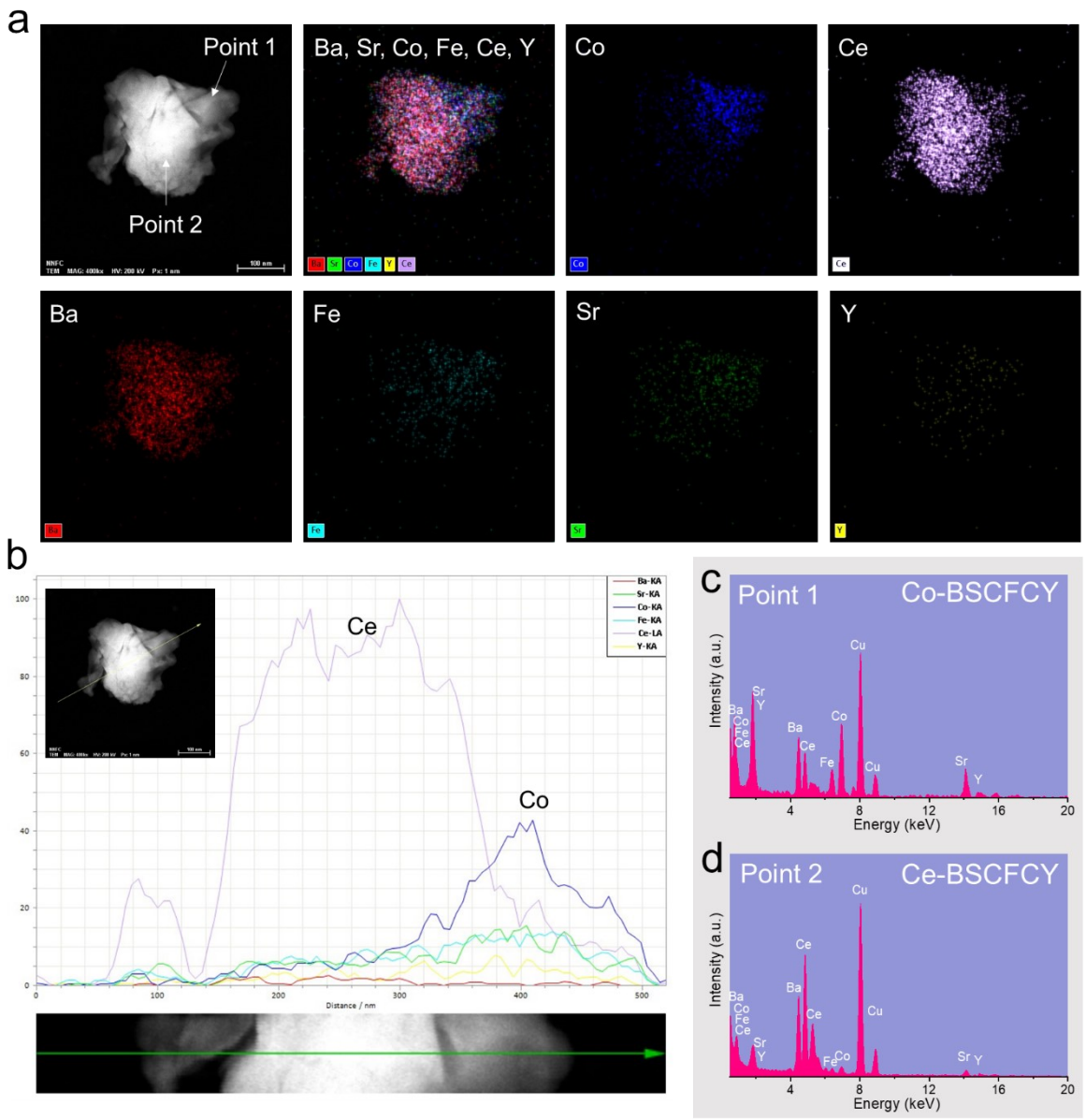

Figure S9. (a) Scanning transmission electron microscopy (STEM) and energy-dispersive X-ray (EDX) analysis of $Ba_{0.5}Sr_{0.5}Co_{0.6}Fe_{0.2}Ce_{0.1}Y_{0.1}O_{3-\delta}$ (BSCFCY) composite. Scale bar = 100 nm. (b) The element profile (Ba, Sr, Co, Fe, Ce, Y) along the scanning line. Point EDX scanning results obtained from (f) point 1 and (g) point 2, respectively.

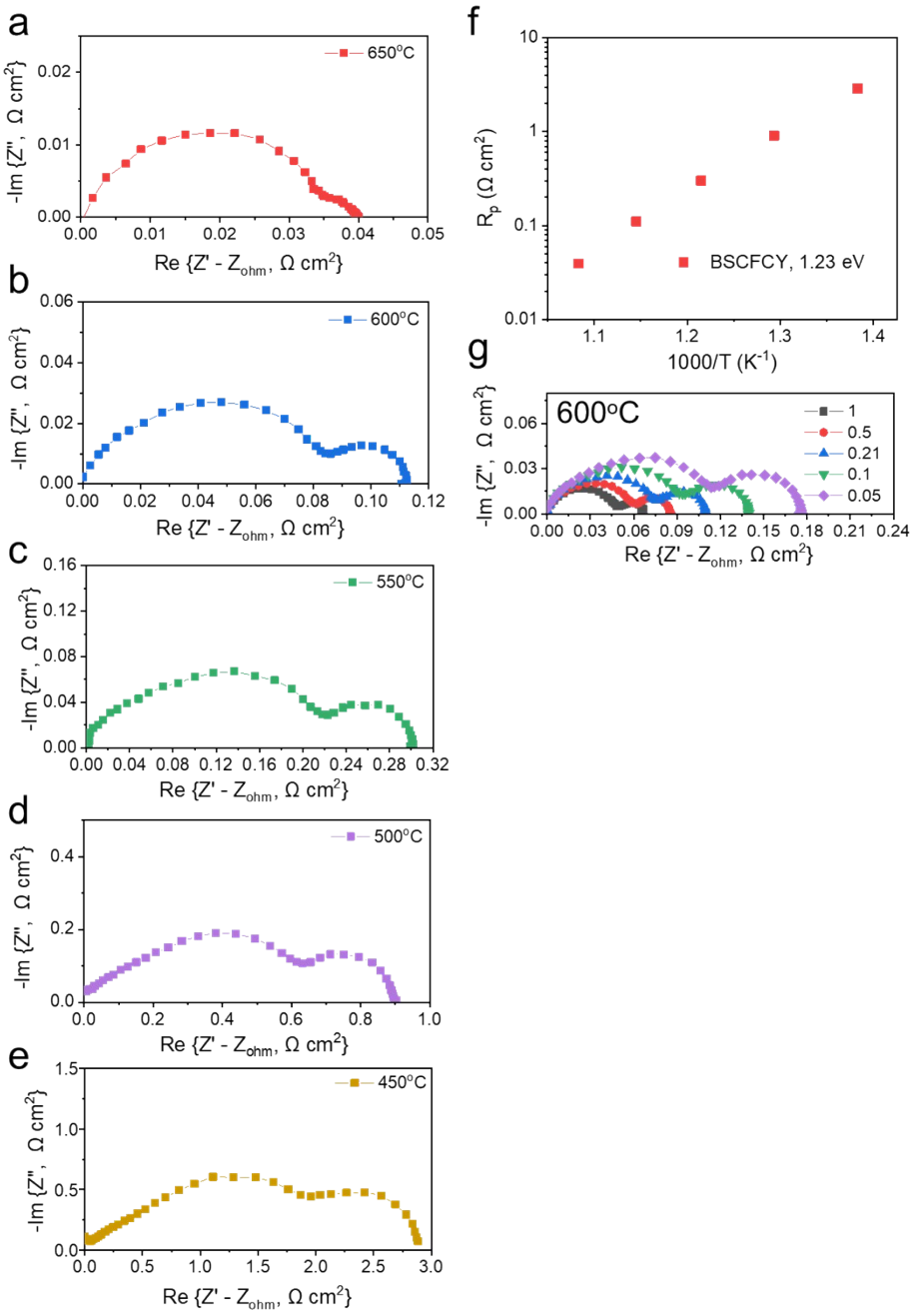

Figure S10. Electrochemical impedance spectroscopy of porous $Ba_{0.5}Sr_{0.5}Co_{0.6}Fe_{0.2}Ce_{0.1}Y_{0.1}O_{3-\delta}$ (BSCFCY) composite cathodes at (a) 650°C, (b) 600°C, (c) 550°C, (d) 500°C, and (e) 450°C, respectively. (f) Arrhenius plot of ASRs. (g) Effect of oxygen partial pressure on ASRs at 600°C.

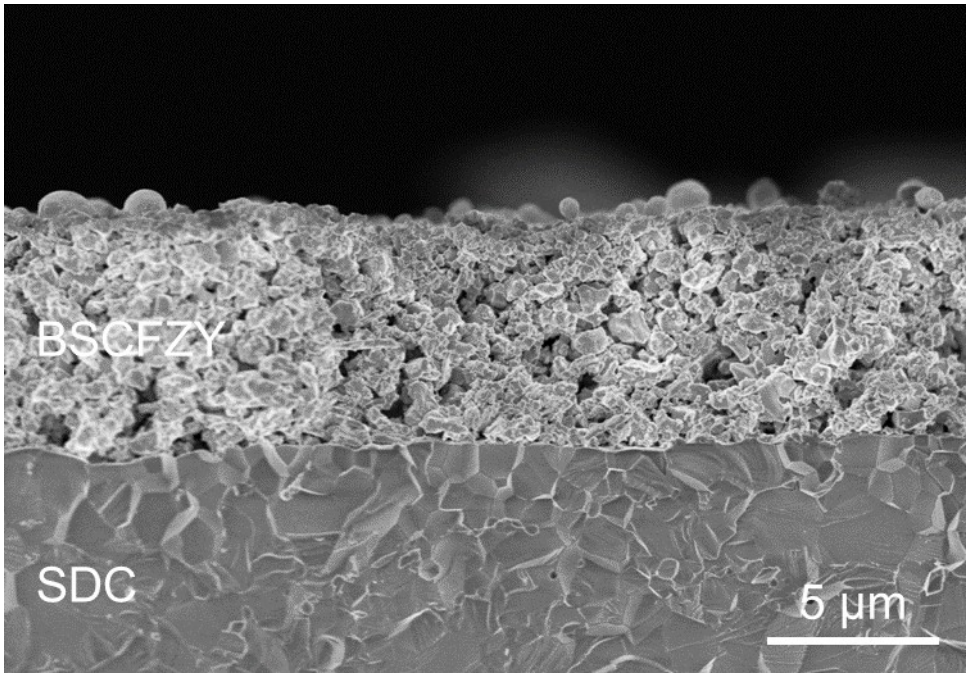

Figure S11. Cross-sectional scanning electron microscopy image of BSCFZY|SDC|BSCFZY symmetric cell.

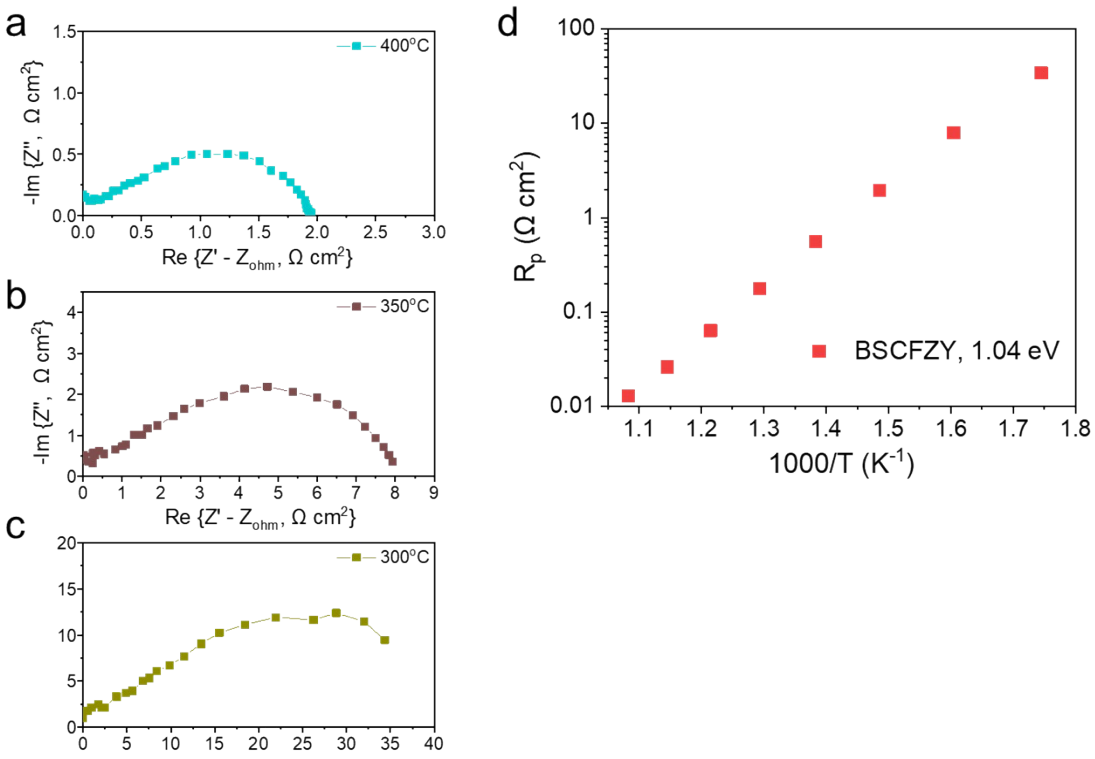

Figure S12. Electrochemical impedance spectroscopy of porous $Ba_{0.5}Sr_{0.5}Co_{0.6}Fe_{0.2}Zr_{0.1}Y_{0.1}O_{3-\delta}$ (BSCFZY) composite cathodes at (a) 400°C, (b) 350°C and (c) 300°C, respectively. (d) Arrhenius plot of ASRs.

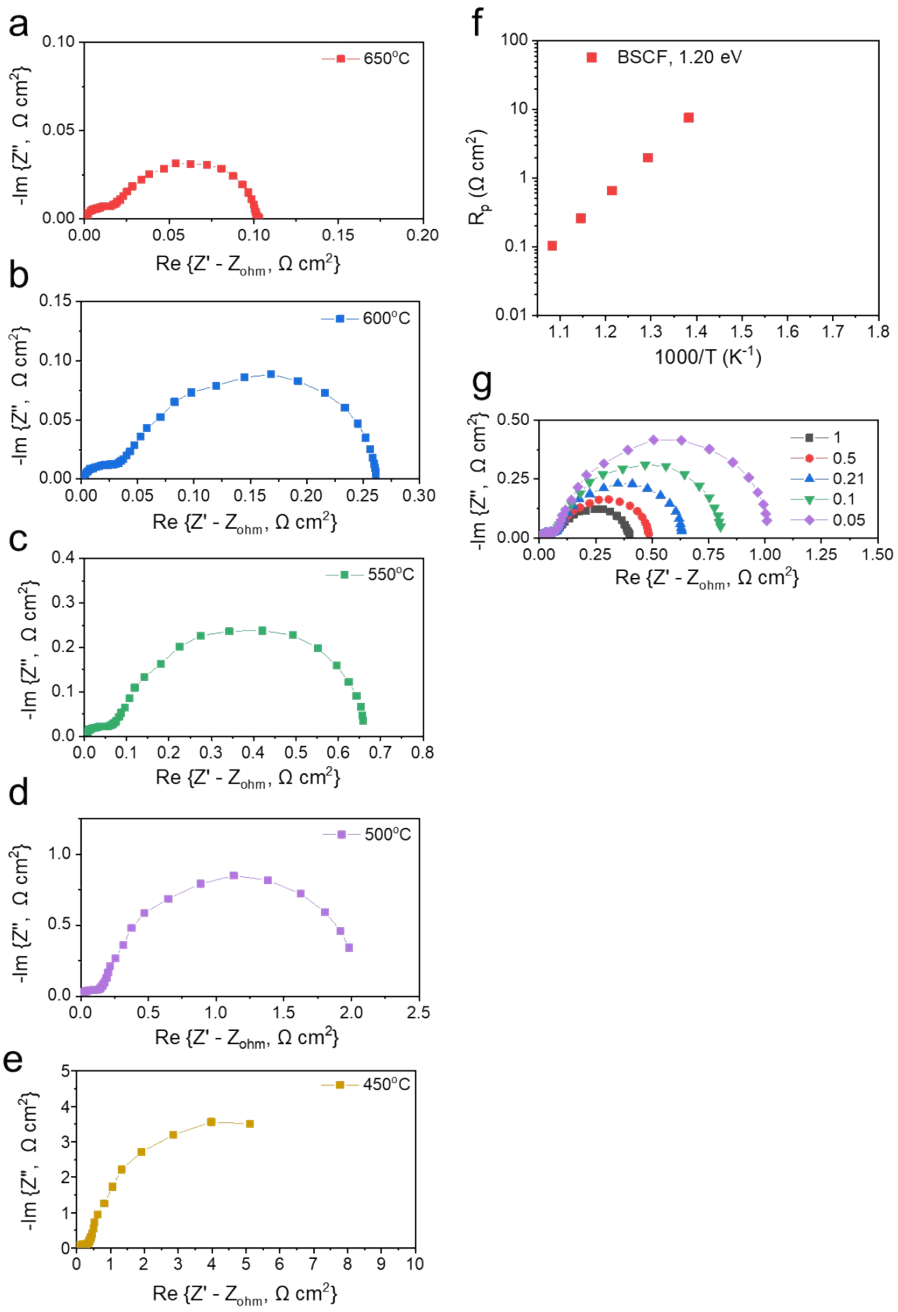

Figure S13. Electrochemical impedance spectroscopy of porous $Ba_{0.5}Sr_{0.5}Co_{0.8}Fe_{0.2}O_{3-\delta}$ (BSCF) cathodes at (a) 650°C, (b) 600°C, (c) 550°C, (d) 500°C, and (e) 450°C, respectively. (f) Arrhenius plot of ASRs. (g) Effect of oxygen partial pressure on ASRs at 550°C.

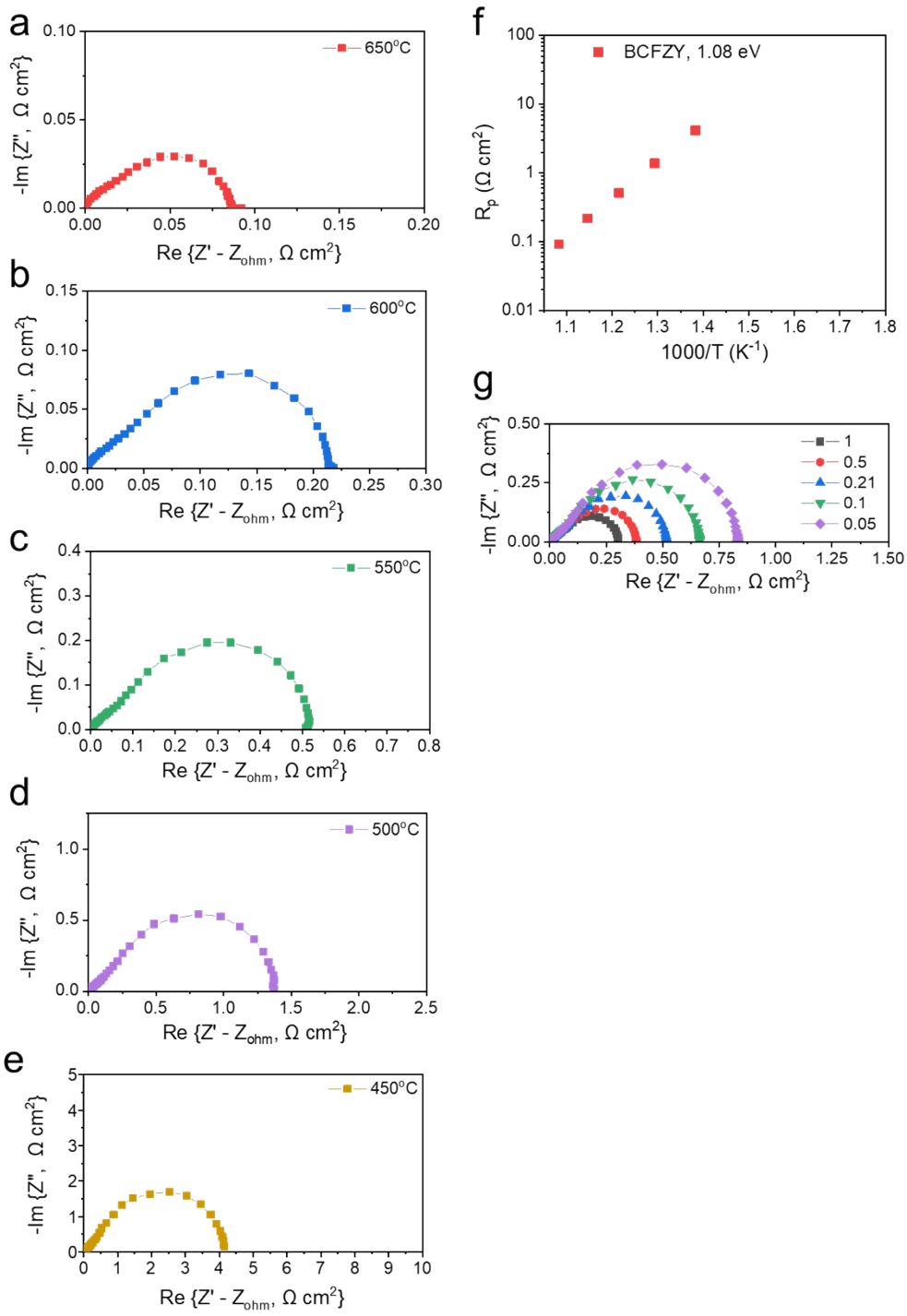

Figure S14. Electrochemical impedance spectroscopy of porous $BaCo_{0.4}Fe_{0.4}Zr_{0.1}Y_{0.1}O_{3-\delta}$ (BCFZY) composite cathodes at (a) 650°C, (b) 600°C, (c) 550°C, (d) 500°C, and (e) 450°C, respectively. (f) Arrhenius plot of ASRs. (g) Effect of oxygen partial pressure on ASRs at 550°C.

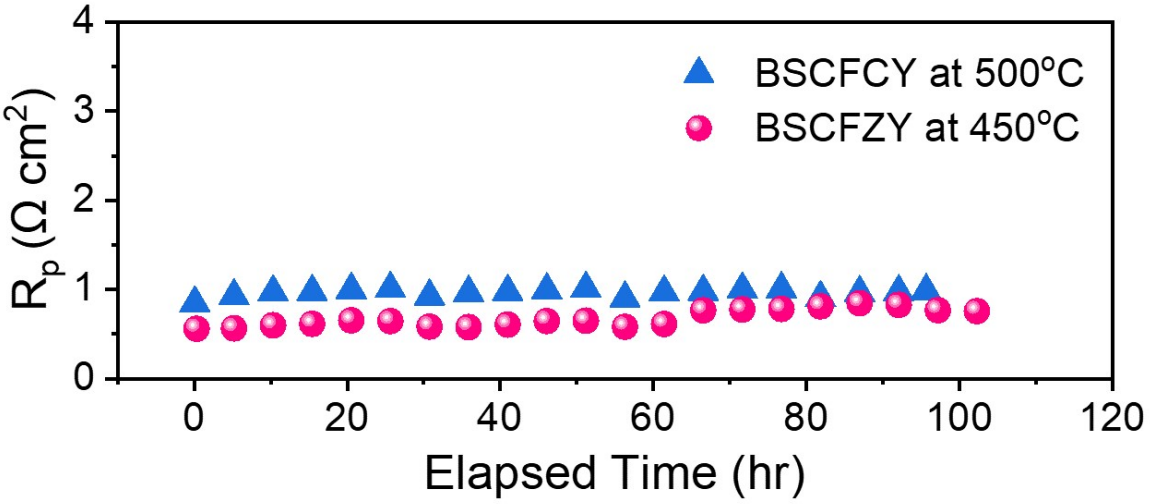

Figure S15. Temporal evolution of polarization resistance of $Ba_{0.5}Sr_{0.5}Co_{0.6}Fe_{0.2}Zr_{0.1}Y_{0.1}O_{3-\delta}$ (BSCFZY) at 450°C and $Ba_{0.5}Sr_{0.5}Co_{0.6}Fe_{0.2}Ce_{0.1}Y_{0.1}O_{3-\delta}$ (BSCFCY) at 500°C.

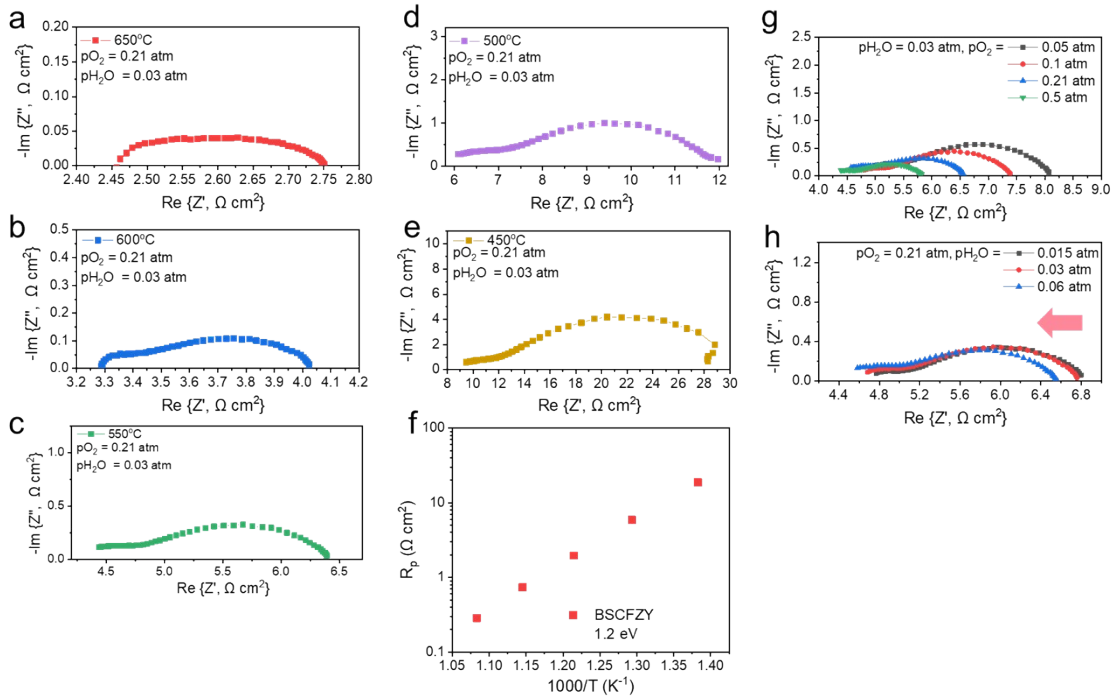

Figure S16. Electrochemical impedance spectroscopy of porous $Ba_{0.5}Sr_{0.5}Co_{0.6}Fe_{0.2}Zr_{0.1}Y_{0.1}O_{3-\delta}$ (BSCFZY) composite cathodes at (a) 650°C, (b) 600°C, (c) 550°C, (d) 500°C, and (e) 450°C, respectively based on proton-conducting electrolytes of $BaZr_{0.1}Ce_{0.7}Y_{0.1}Yb_{0.1}O_{3-\delta}$ (BZCYYb) (f) Arrhenius plot of area-specific-resistances (ASRs). (g) Effect of oxygen partial pressure on ASRs at 550°C. (h) Effect of water vapor pressure on ASRs at 550°C

Table S2. Summary of electronic conductivity, oxygen ion conductivity, and transference number of oxygen ion ($t_{O^{2-}}$) of BSCF and BCFZY at 600°C

Material	Electronic conductivity (S cm^{-1})	Oxygen ion conductivity (S cm^{-1})	$t_{O^{2-}}$
BSCF	~45[11]	0.006[24]	1.33 x 10^{-4}
BCFZY	~1.25[11]	0.018[25]	1.44 x 10^{-2}

Hypothetically, it is expected that the phase with a high Co concentration will have more electronic conductivity, while those with high Zr concentration will have more oxygen ionic conductivity due to the larger lattice parameter. Here, as the composition of Co-rich and Zr-rich phase in BSCFZY closely approximate the corresponding compositions found in BSCF and BCFZY, we searched the literatures to estimate the characteristic electronic & ionic conductivity of individual phases of Co-BSCFZY and Zr-BSCFZY. Shown in Table S2 is a summary of electronic conductivity, oxygen ion conductivity and transference number of oxygen ion ($t_{O^{2-}}$) of BSCF and BCFZY at 600°C.

According to Table S2, the electronic conductivity of BSCF is approximately 36 times higher than that of BCFZY, as implied by its higher B-site Co concentration (i.e., BSCF: 80mol% BCFZY: 40mol%). However, the oxygen ion conductivity is found to be nearly three times higher in BCFZY; according, the oxygen transference number is ~100 times higher. Due to the substitution of Co^{3+} by the larger Zr^{4+} and Y^{3+} cations,[14] BCFZY shows a larger lattice parameter (BCFZY: ~4.09 Å) than BSCF (3.98 Å)[15] and thus possesses a larger free volume, which is commonly associated with increased oxygen mobility and decreased activation energy in perovskites.[16,17]

In light of above findings, we conjecture the following characteristic electron-hole & ionic conducting pathway in BSCFZY composite: Stronger electron-hole conduction in Co-rich phase and stronger oxygen ion conduction in Zr-rich phase.

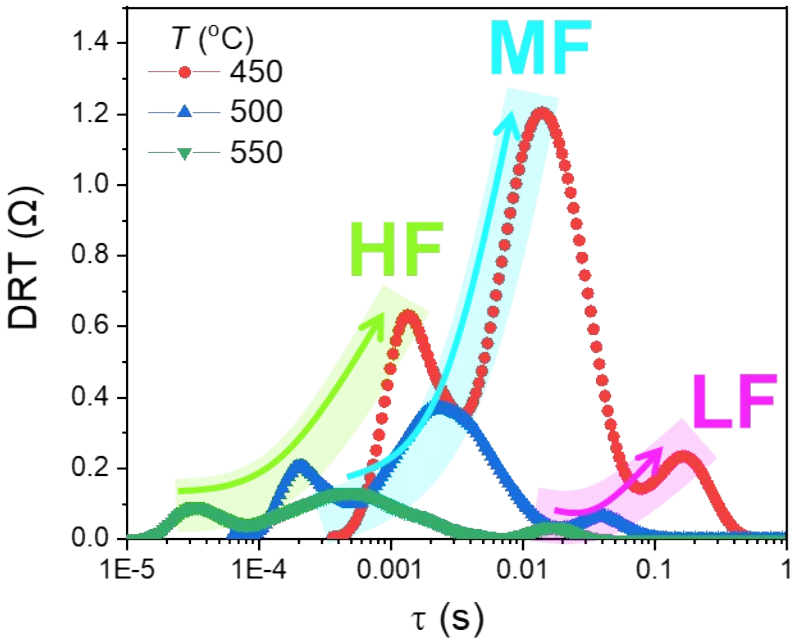

Figure S17. Temperature dependence of DRT plots of $Ba_{0.5}Sr_{0.5}Co_{0.6}Fe_{0.2}Zr_{0.1}Y_{0.1}O_{3-\delta}$ (BSCFZY) electrodes.

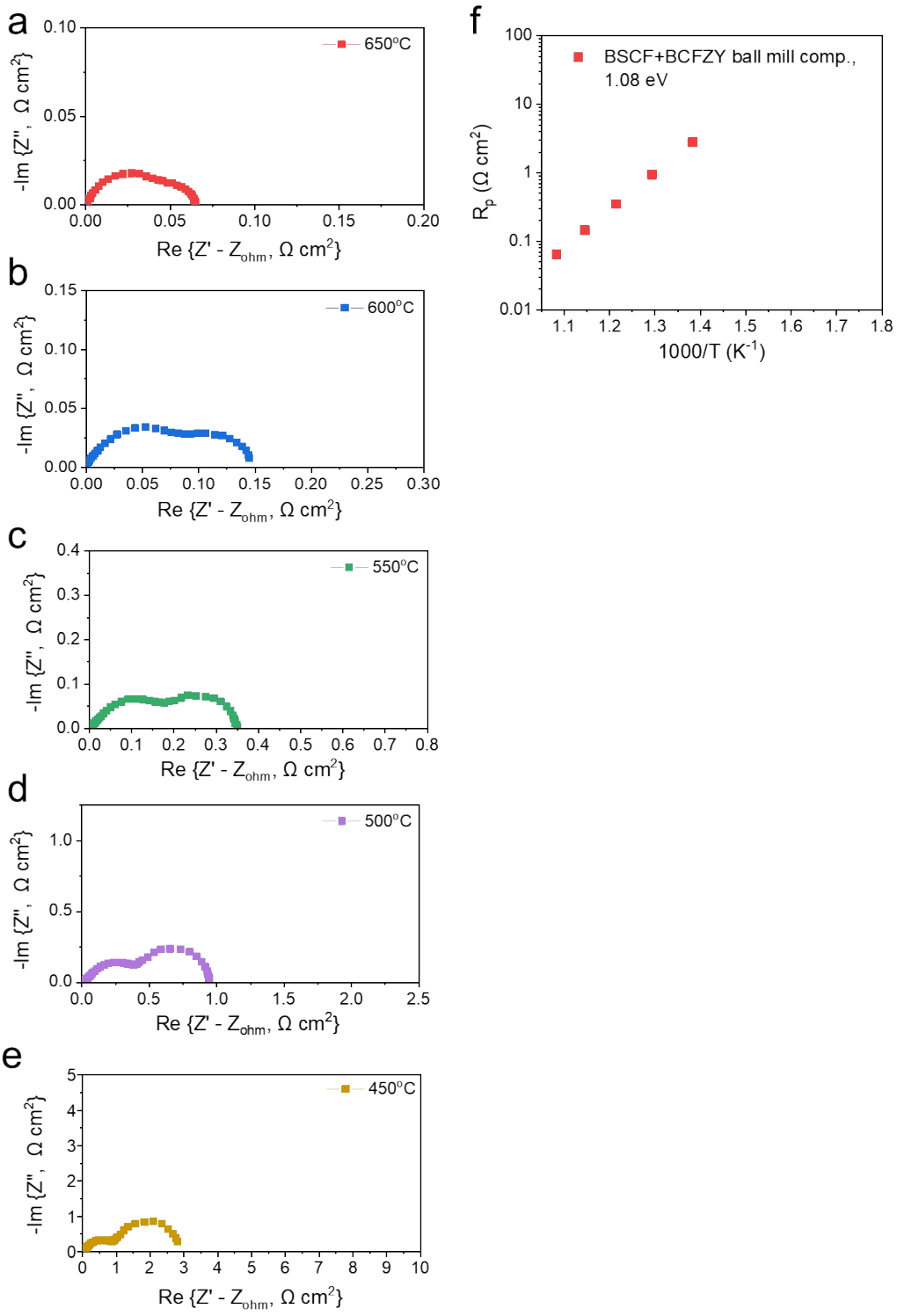

Figure S18. Electrochemical impedance spectroscopy of ball-mill $Ba_{0.5}Sr_{0.5}Co_{0.8}Fe_{0.2}O_{3-\delta}$ (BSCF) + $BaCo_{0.4}Fe_{0.4}Zr_{0.1}Y_{0.1}O_{3-\delta}$ (BCFZY) composite cathodes at (a) 650°C, (b) 600°C, (c) 550°C, (d) 500°C, and (e) 450°C, respectively. (f) Arrhenius plot of ASRs.

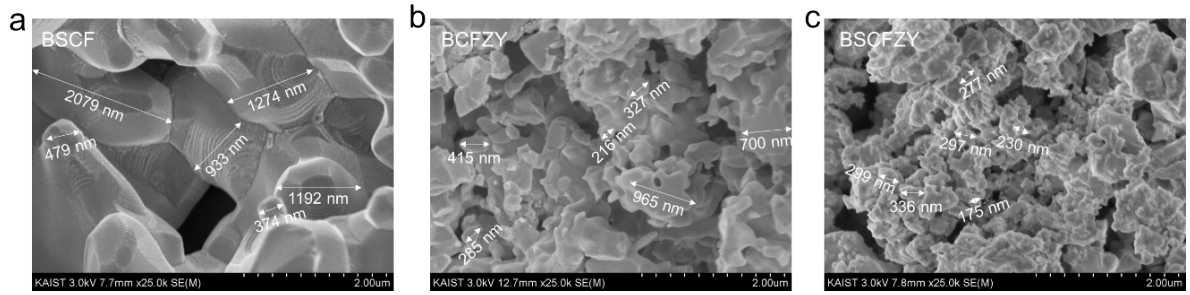

Figure S19. SEM images of (a) BSCF, (b) BCFZY and (c) BSCFZY to compare the grain size.

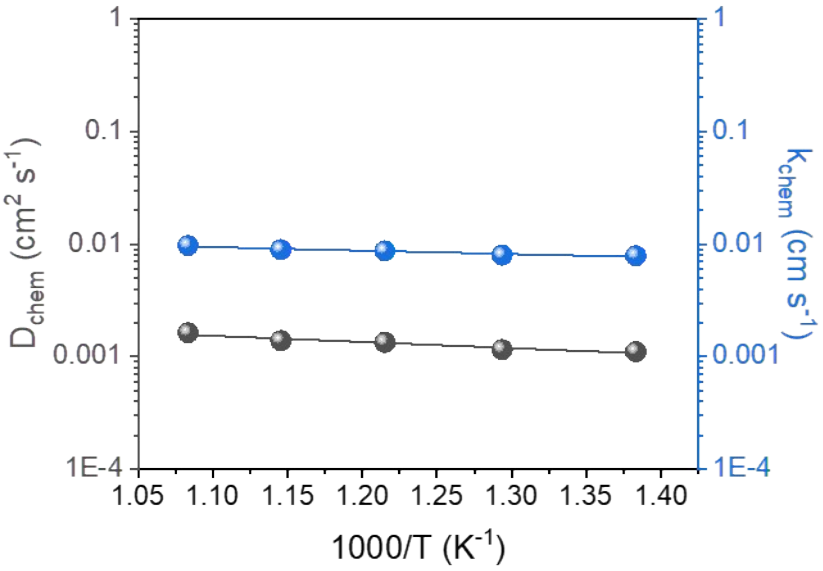

Figure S20. Arrhenius plots of the D_{chem} and K_{chem} for $Ba_{0.5}Sr_{0.5}Co_{0.6}Fe_{0.2}Zr_{0.1}Y_{0.1}O_{3-\delta}$ (BSCFZY) extracted from electrical conductivity relaxation method.

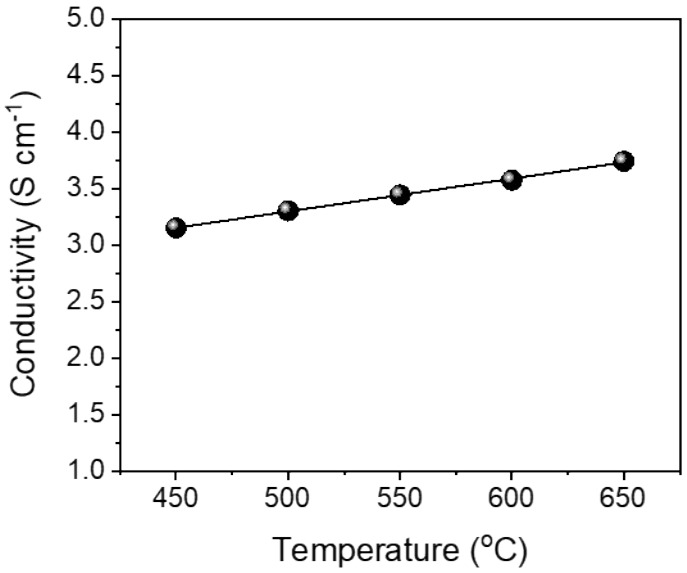

Figure S21. Electronic conductivity of $Ba_{0.5}Sr_{0.5}Co_{0.6}Fe_{0.2}Zr_{0.1}Y_{0.1}O_{3-\delta}$ (BSCFZY).

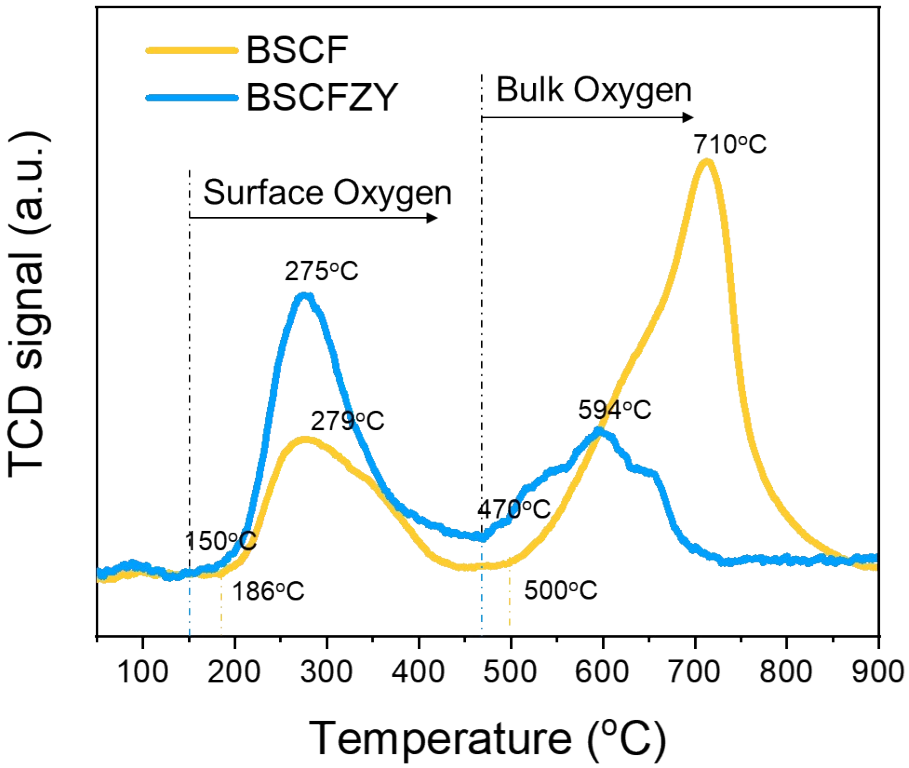

Figure S22. O_2-TPD profiles of BSCF and BSCFZY

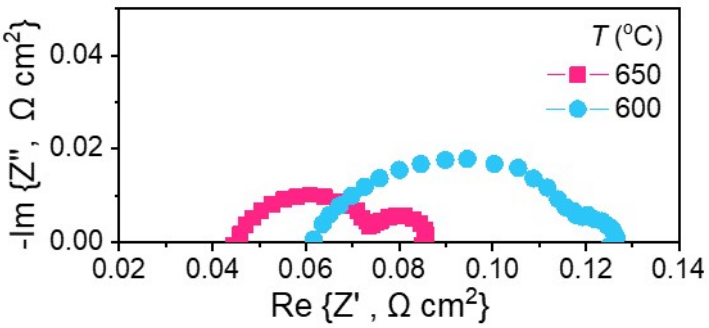

Figure S23. (a) Electrochemical impedance spectroscopy (EIS) of Ni-GDC|GDC|BSCFZY button cell at different temperatures.

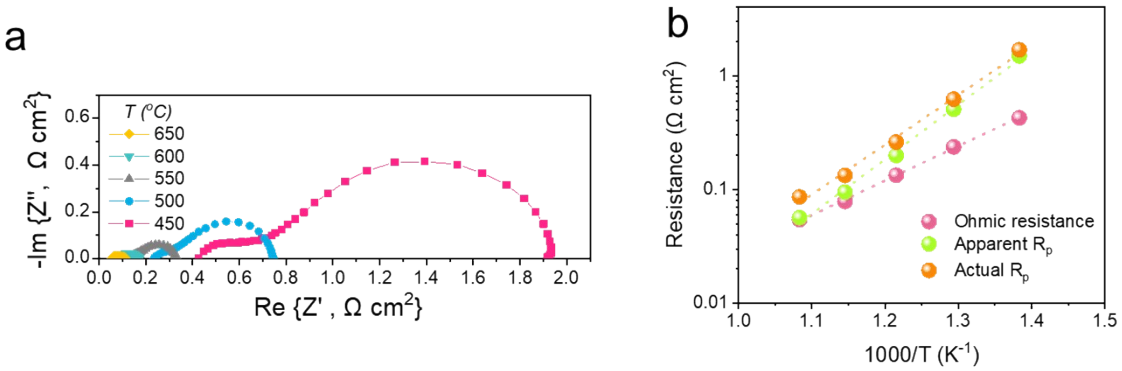

Figure S24. (a) Electrochemical impedance spectroscopy (EIS) of Ni-SDC|SDC|BSCFZY button cell at different temperatures. (b) Arrhenius plots of electrode and electrolyte resistance of the button cell.

According to the literature,[18] the actual interfacial polarization resistance on mixed-conducting electrolytes can be calculated using the following equation:

$$R_p = \frac{R_T - R_b}{\frac{V_{OC}}{E_N}\left[1 - \frac{R_b}{R_T}\left(1 - \frac{V_{OC}}{E_N}\right)\right]}$$

where R_p is the polarization resistance (Ω cm^2), R_T is the total resistance (Ω cm^2), R_b is the resistance of the bulk electrolyte (Ω cm^2), V_{oc} is the open-circuit voltage (V), and E_N is the Nernst potential(V).

Accordingly, the actual R_p values can be calculated as shown in Table S3.

Table S3. Electrochemical characteristics of Ni-SDC|SDC|BSCFZY cell under open-circuit conditions.

T(°C)	R_T	R_b	V_{oc}	E_N	R_p
650	0.11067	0.0541	0.84	1.121	0.086
600	0.17309	0.07827	0.89	1.127	0.133
550	0.33199	0.1333	0.93	1.133	0.261
500	0.74133	0.23653	0.97	1.139	0.622

450	1.91626	0.42608	1.03	1.145	1.69

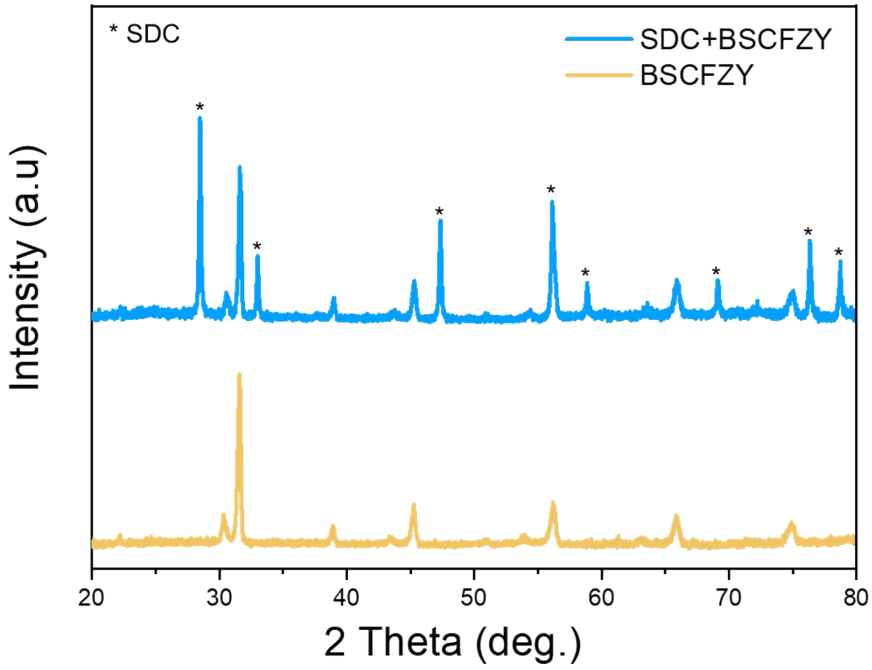

Figure S25. Thermal compatibility test between $Sm_{0.2}Ce_{0.8}O_{2-\delta}$ (SDC) and $Ba_{0.5}Sr_{0.5}Co_{0.6}Fe_{0.2}Zr_{0.1}Y_{0.1}O_{3-\delta}$ (BSCFZY) conducted at 600°C for 10 hours under stagnant air.

Table S4. Summary of the cathode, single cell configuration, peak power density, degradation rate, fabrication process and thermal cycling outcomes for recent solid oxide fuel cells based on self-assembled nano-composites. Note: BSCFZY ($Ba_{0.5}Sr_{0.5}Co_{0.6}Fe_{0.2}Zr_{0.1}Y_{0.1}O_{3-\delta}$), c-SYNC (composite of $SrNb_{0.1}Co_{0.9}O_{3-\delta}$ and $Y_2W_3O_{12}$), SLC-SZC ($Sr_{0.8}La_{0.2}Co_{0.8}Zr_{0.2}O_{3-\delta}$), BZC-BC ($BaZr_{0.6}Co_{0.4}O_{3-\delta}$), LSM-ESB ($La_{1-x}Sr_xMnO_3$-$Bi_{1.6}Er_{0.4}O_3$), SCFN ($Sr_{0.9}Ce_{0.1}Fe_{0.8}Ni_{0.2}O_{3-\delta}$), LSCF-PBCC ($PrBa_{0.8}Ca_{0.2}Co_2O_{5+\delta}$ infiltrated $La_{0.6}Sr_{0.4}Co_{0.2}Fe_{0.8}O_3$).

Cathode	Single cell configuration	Peak power density (W cm^{-2})	Long-term testing (Degradation rate)	Fabrication process	Thermal cycling
BSCFZY (our work)	Ni-GDC10|GDC20|BSCFZY	1.29 @650°C 1.10 @600°C	~310 hr (0%/100hr)	Sol-gel one pot synthesis	○
	Ni-SDC|SDC|BSCFZY	1.09 @650°C			
c-SYNC[1]	Ni-YSZ|YSZ|SDC|c-SYNC	0.817 @650°C	200 hr (~1.8%/100hr)	Multi-step compositing	△ (Based on half-cell)
SLC-SZC[2]	Ni-YSZ|YSZ|GDC|SLC-SZC	1.038 @600°C	×	Glycine-nitrate combustion	×
BZC-BC[3]	Ni-YSZ|YSZ|GDC|BZC-BC	1.094 @650°C 0.74 @600°C	~25 hr (~13.0%/100hr)	Glycine-nitrate combustion	×
LSM-ESB[4]	Ni-YSZ|YSZ|ESB|LSM-ESB	~1.04 @650°C ~0.55 @600°C	×	Glycine-nitrate combustion	×
SCFN[5]	Ni-SDC|SDC|SCFN	1.208 @650°C 0.977 @600°C	~560 hr (1.96%/100hr)	Sol-gel one pot synthesis	×
LSCF-PBCC[6]	Ni-GDC|GDC|LSCF-PBCC	1.22 @600°C	~250 hr (0%/100hr)	Infiltration	×